Magma mingling/mixing at Citlaltépetl volcano, eastern Trans-Mexican Volcanic Belt, and the plumbing system during the ~5 ky BP Jamapa explosive eruption

Arce, José Luis; Macías, José Luis; González-Herrera, Mireya; Caricchi, Luca; Miranda Muruzabal, Martin; Sourisseau, Delphine; Avellán, Denis R.; Torres-Orozco, Rafael

How to cite

ARCE, José Luis et al. Magma mingling/mixing at Citlaltépetl volcano, eastern Trans-Mexican Volcanic Belt, and the plumbing system during the ~5 ky BP Jamapa explosive eruption. In: Lithos, 2025, vol. 522-523, p. 108388. doi: 10.1016/j.lithos.2025.108388

This publication URL: https://archive-ouverte.unige.ch/unige:190044
Publication DOI: 10.1016/j.lithos.2025.108388

LITHOS 522–523 (2026) 108388

Contents lists available at ScienceDirect

LITHOS

journal homepage: www.elsevier.com/locate/lithos

Magma mingling/mixing at Citlaltépetl volcano, eastern Trans-Mexican Volcanic Belt, and the plumbing system during the ~5 ky BP Jamapa explosive eruption

José Luis Arce [a,*], José Luis Macías [b], Mireya González-Herrera [c], Luca Caricchi [d], Martin Miranda [d], Delphine Sourisseau [e], Denis R. Avellán [f], Rafael Torres-Orozco [g]

[a] Instituto de Geología, Universidad Nacional Autónoma de México, Ciudad Universitaria Coyoacán, Ciudad de México, Mexico
[b] Instituto de Geofísica, Universidad Nacional Autónoma de México, Antigua Carretera a Pátzcuaro 8701, Morelia, Michoacán, Mexico
[c] Escuela Superior de Ingeniería y Arquitectura, Instituto Politécnico Nacional, Ticomán, Ciudad de México, Mexico
[d] Department of Earth Sciences, University of Geneva, Geneva, Switzerland
[e] Postdoctoral Fellow SECIHTI - Instituto de Geología, Universidad Nacional Autónoma de México, Ciudad Universitaria Coyoacán, Ciudad de México, Mexico
[f] SECIHTI - Instituto de Geofísica, UNAM, Campus Morelia, Morelia, Michoacán, Mexico
[g] Instituto de Geociencias, Universidad Nacional Autónoma de México, Campus Juriquilla, Juriquilla, Querétaro, México

ARTICLE INFO

Keywords:
Citlaltépetl volcano
Explosive eruptions
Holocene volcanism
Magma mixing/mingling
Geothermobarometry

ABSTRACT

The active Citlaltépetl volcano (Pico de Orizaba) located in the eastern part of the Trans-Mexican Volcanic Belt, is the highest mountain (5636 masl) in Mexico and North America. Intense explosive and effusive activity took place in the Holocene (mainly with VEI < 5), with some volcanic eruptions that have not yet been described, like the Jamapa Pyroclastic Flow deposit. Jamapa deposits were emplaced up to 4 km from the summit on the northern flank of the volcano, and rest on a paleosol dated at ~5 ky BP. The deposits consist of subrounded to rounded >30 cm-diameter porphyritic clasts of dacitic pumice (63.6 wt% SiO_2), andesitic scoria (58.9 wt% SiO_2), banded vesicular clasts (59.0 wt% SiO_2), andesitic dense volcanic bombs (62.8 wt% SiO_2), and magmatic crystalline enclaves (64.0 wt% SiO_2). The pumice contains plg + opx + cpx ± Fe-Ti oxides, and rare amph phenocrysts, whilst the scoria and banded clasts contain opx + cpx + amph + plag +/− Fe-Ti oxides. Glass matrix in all samples of the Jamapa Pyroclastic Flow a large compositional range is recorded (dacite to rhyolite; 66.6–78.2 wt% SiO_2), and plagioclase is also heterogeneous ($An_{23.3}$ to An_{78}), whereas pyroxene and amphibole are almost homogeneous in all samples. Cpx-liquid and amphibole geothermometry of the Jamapa juvenile components show significant differences among samples: andesitic scoria (900–946 °C), the pumice barren of amphibole (930 °C), and the banded sample (970–986 °C). On the other hand, the "MagMaTaB" liquid geothermobarometer model yielded 884 °C for the scoria, 934 °C for the banded, and 898 °C for the pumice samples. P-T results suggest the occurrence of at least two magmatic reservoirs beneath the volcano: a deep (~20 km), relatively mafic, and volatile-rich reservoir and a shallow (~8 km) reservoir with a felsic, stagnant magma. These results and the heterogeneous composition of the glass matrix and plagioclase crystals suggest that not only mingling but also mixing occurred during the Jamapa volcanic event. We conclude that a mafic magma stored at a depth of ~20 km ascended to reach the dacitic reservoir located ~8 km below the volcano, where both magmas were partially mixed, provoking overpressure of the system and eventually triggering the explosive eruption, destroying a pre-existing dome.

1. Introduction

Explosive volcanic eruptions are the most dangerous natural phenomena worldwide, especially for more than 80 million people around the world living in active volcanic areas (Doocy et al., 2013). Mitigation of volcanic hazards is a key point to avoid catastrophic effects of volcanic events like the 79 CE eruption of Vesuvius volcano in Italy (Luongo et al., 2003) or the 1902 Mount Pelée eruption, Martinique (Gueugneau

* Corresponding author.
E-mail address: jlarce@Geologia.unam.mx (J.L. Arce).

https://doi.org/10.1016/j.lithos.2025.108388
Received 4 August 2025; Received in revised form 19 December 2025; Accepted 20 December 2025
Available online 26 December 2025

et al., 2020), with thousands of deaths. To avoid these kinds of disasters, it is of great importance to know the volcanic systems, either by geophysical or petrological studies (Cioni et al., 2021). Anticipating volcanic activity requires multidisciplinary investigations, such as initial studies of volcanic history, geophysical and petrological analyses of the plumbing system beneath it, as well as monitoring programs (Magee et al., 2018). By studying the volcanic deposits to determine areal distribution, composition, volume, is important to define the eruptive styles recorded in the volcano life, but the composition, pressure, temperature, and volatile contents are also crucial parameters (Cashman et al., 2017; Yamamoto et al., 2021). Recent magmatic plumbing system models consider open and vertical extent systems (e.g.: Cashman and Giordano, 2014) which can remain for a long time and develop crystal mushes (Cooper and Kent, 2014). Such low-melt bodies can be partially melted and periodically remobilized by hotter and mafic magmas (Bachmann and Bergantz, 2006). A volcanic eruption can take place If enough magma is injected into the reservoir to modify its physico-chemical characteristics, such as viscosity and density, and ascend to the surface (Caricchi et al., 2021). Magma mixing/mingling is a common phenomenon that takes place in volcanic systems (Sparks et al., 1977; Morgavi et al., 2022). It happens when a magma batch, commonly hotter, crystal-poor, volatile-rich, and more mafic, is injected into a shallower reservoir where a colder, evolved, and volatile-poor magma is hosted. Mingling is referred to as a mechanical mix between two magmas; in contrast, mixing occurs when chemical interaction between two magmas takes place (Morgavi et al., 2022), although a continuous spectrum between mixing and mingling exists. Such injection produces a temperature increase, lowers the viscosity, and over pressurizes the host magma, capable of triggering a volcanic eruption (Eichelberger and Izbekov, 2000; Huber et al., 2011). This is the case of the eruption that dispersed the Jamapa Pyroclastic Flow on the northern flank of Citlaltépetl volcano.

In this work, we study a pyroclastic density current defined as the Jamapa Pyroclastic Flow, from Citlaltépetl volcano, located in the eastern Trans-Mexican Volcanic Belt (TMVB) (Fig. 1). Field observations, combined with whole-rock chemistry, and microprobe analysis of mineral phases, permitted us to propose that two different magmas partially mixed (mingling/mixing) just before eruption, generated an explosive event that produced the Jamapa Pyroclastic Flow deposit. Additionally, we used different geothermobarometers to constrain, for the first time, the magmatic plumbing system of this active volcano.

2. Geology background and eruptive history

Citlaltépetl is classified as an active volcano (Crausaz, 1994) in a quiescent state that represents the highest mountain of Mexico (5636 m above sea level; masl; and 3850 m high relative to the east side). The volcano lies at the southernmost edge of the N-S aligned Cofre de Perote-Las Cumbres-Pico de Orizaba volcanic range, on the eastern TMVB. Citlaltépetl volcano is related to the subduction of the Cocos plate beneath the North American plate (Fig. 1). It lies 400 km from the Middle America trench, with the slab located at a depth of 200 km below the volcano (Pérez-Campos et al., 2008). Volcanic activity in the TMVB province started in the early Miocene (Ferrari et al., 2012; Lenhardt et al., 2010; Arce et al., 2020) and continues in the present, dominated by calc-alkaline andesitic to dacitic products (Gómez-Tuena et al., 2007). Citlaltépetl was constructed on a Mesozoic sequence constituted by: 1) Metamorphic rocks (green schists) and granodioritic rocks (Campos-Enríquez and Garduño-Monroy, 1987; Gómez-Alvarez et al., 2021), and 2) A continental sedimentary sequence of Jurassic age plus marine limestones of the Sierra Madre Oriental province of Cretaceous age (Campos-Enríquez and Garduño-Monroy, 1987; Gómez-Alvarez et al., 2021) (Fig. 2).

Two previous stratovolcanoes were built before the Citlaltépetl edifice (Fig. 3). The oldest one, called Torrecillas, was constructed by basalt and basaltic andesite lavas between ~650 ka and ~ 210 ka (Carrasco-Núñez et al., 2021; Höskuldsson and Robin, 1993). Torrecillas was destroyed by a volcanic sector collapse that generated a debris avalanche dispersed to the north toward the Jamapa ravine (Carrasco-Núñez and Rose, 1995). Remnants of Torrecillas edifice can be observed in the south flank of the current Citlaltépetl volcano. Since 210 ka, a new volcano called Espolón de Oro began its construction, which was dominated by andesitic to dacitic products (Carrasco-Núñez, 2000). Espolón de Oro also recorded a sector collapse that partially destroyed

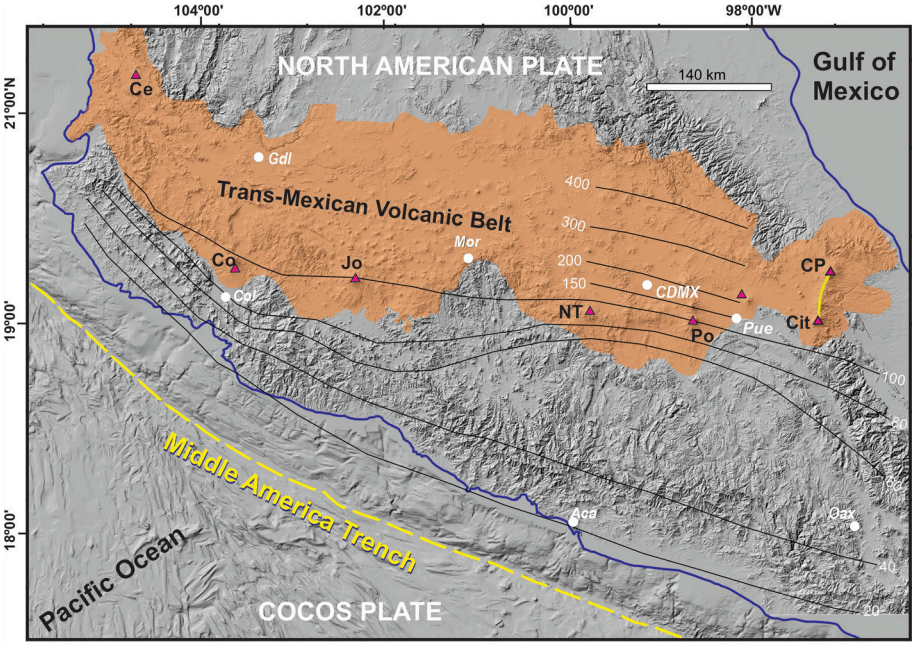

Fig. 1. Location of the Citlaltépetl volcano (Cit) in the eastern Trans-Mexican Volcanic Belt province. Some volcanic structures: Cofre de Perote (CP), Popocatépetl (Po), Nevado de Toluca (NT), Tancítaro (Ta), Colima (Co), and Ceboruco (Ce), and cities: Oaxaca (Oax), Acapulco (Aca), Mexico City (CDMX), Morelia (Mor), Colima (Col), and Guadalajara (Gdl) are shown. Contour black lines represent depths of the subducted Cocos slab (Pérez-Campos et al., 2008). The continuous yellow line represents the Cofre de Perote-Pico de Orizaba volcanic range.

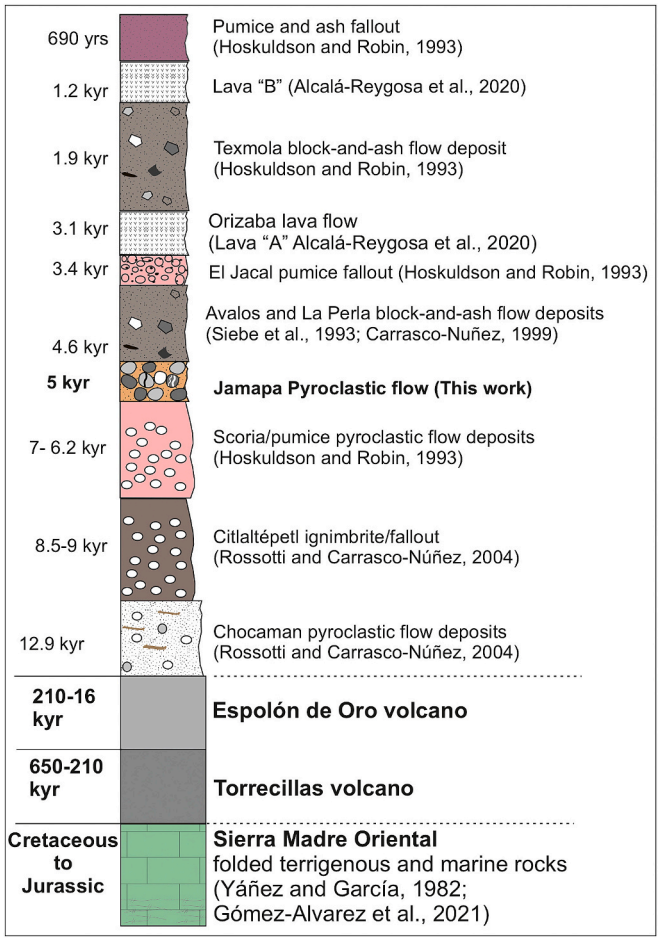

Fig. 2. General stratigraphy of the Citlaltépetl volcano based on previous works. Ages are in years before present.

the volcanic structure some 16 ka, with the emplacement of a debris avalanche and associated lahars to the NE (Carrasco-Núñez et al., 1993). Remnants of the Espolón de Oro edifice can be observed in the north of the current Citlaltépetl volcano (Fig. 3). Finally, the construction of the Citlaltépetl edifice started around 16 ka and continues to the present, driven by numerous explosive and effusive eruptions that produced magmas with diverse compositions (basaltic andesite to dacite; Höskuldsson and Robin, 1993; Schaaf and Carrasco-Núñez, 2010). One of the most important explosive events is the Citlaltépetl Plinian eruption, which happened between ~9000 and 8500 yr BP (Rossotti and Carrasco-Núñez, 2004; Vásquez-Montoya et al., 2025).

During the growth of the Citlaltépetl cone, several nearby dome complexes were emplaced, including the Malacara Dacite, North Dome, and Chichimeco Dome Complex (Carrasco-Núñez, 2000). The stratigraphic record highlight some recent explosive and effusive activity with the emission of two dacitic lava flows emplaced on the southwestern flank of the volcano (defined as Lava A and Lava B) dated by cosmogenic ^{36}Cl at 3.0 and 1.1 ky BP, respectively (Alcalá-Reygosa et al., 2020), as well as an explosive eruption dated at 690 yr BP (Höskuldsson and Robin, 1993) that emplaced a pumice fall deposit. In addition, historical explosive activity has been reported between 1537 and 1687 CE (e.g., Mooser et al., 1958; Höskuldsson and Robin, 1993).

Despite all these investigations on the stratigraphy of Citlaltépetl volcano, some events have not been studied and/or described in detail, mainly because they outcrop in inaccessible areas (high altitudes, not too many roads, etc.), like the Jamapa Pyroclastic Flow deposit, the subject of this paper.

3. Methodology

3.1. Field sampling

Many samples were taken in an area of 50 m^2 in the most complete outcrop (the star in Fig. 1A). Some samples were selected to perform petrography, chemical composition, and microprobe analyses: three pumice fragments, two banded fragments, two black scoria fragments, two dense volcanic bombs, and two microgranular crystalline fragments. Juvenile constituents are clearly the vesicular fragments (pumice, scoria, and banded samples), most of them are subrounded, sometimes with cauliflower structures and poor crystalline. Whereas the dense volcanic bombs look very fresh, gray in color, sometimes with bread-crust structures, glass-rich matrix, and sometimes with a vesiculated core (Fig. 5C). These characteristics of the dense volcanic bombs suggest they could be juvenile, or at least, very close in time with the Jamapa Pyroclastic Flow event. Microgranular fragments are also common, varying in color, grain-size, and texture, completely made of crystals of plagioclase, amphibole, and pyroxene, suggesting they were solidified at depth.

3.2. Whole-rock chemical analysis

Eleven samples were selected for whole-rock chemical analysis. Samples were cleaned with distilled water and then dried in an oven for 24 h at 80 °C. Then, samples were powdered in a HERZOG pulverizing mill with a grinding vessel made of chromium steel for 2 min in the Instituto de Geología (IGL), UNAM. Major element compositions were measured with X-Ray Fluorescence spectrometry (XRF) using a RIGAKU ZSX PRIMUS II wavelength dispersive sequential spectrometer at the X-Ray Fluorescence Laboratory, LANGEM from IGL, following the methodology detailed on the laboratory website (https://langem.Geología.unam.mx/laboratorios/laboratorio-de-fluorescencia-de-rayos-x/). Trace elements were measured by Inductively Coupled Plasma Mass Spectrometry (ICP-MS) using a Thermo iCAP Q spectrometer at the Ultraclean and ICP-MS Laboratory from the Instituto de Geociencias, UNAM, Juriquilla, Queretaro, following the methodology described by Mori et al. (2007).

3.3. Microprobe analysis

Microprobe analyses were performed on each sample type (scoria, pumice, banded, dense volcanic bomb, and crystalline enclave with a JEOL JXA8900-R electron probe microanalyzer (EPMA), equipped with five spectrometers, at Laboratorio Universitario de Petrología (LUP), UNAM, Mexico City. The operating conditions used for feldspar were an accelerating voltage of 20 kV, a beam current of 20 nA, with a focused beam. All the other phases (amphibole, pyroxene, and glass) were analyzed using a 10 nA beam current with a 15 kV accelerating voltage. Pyroxene and amphibole were analyzed with a focused beam of 1 μm in size, counting by 30 s for all elements, except Na and K that is 10 s for amphibole crystals. Whereas glass was measured with a defocused beam of 10 μm to minimize sodium migration (Nielsen and Sigurdsson, 1981).

4. Results

Only restricted outcrops of the Jamapa Pyroclastic Flow have been found in the northern slopes of Citlaltépetl volcano at altitudes around 4178 masl. The best exposures are located 4 km from the summit. The deposit can be easily recognized because many blocks are sparsed on the surface with subrounded shapes of scoriaceous and banded structures, together with dense volcanic bombs with breadcrust structures (Fig. 3). The deposit, reaching 80 cm in thickness and rests on an oxidized paleosol (at least 40 cm thick), rich in organic matter that was sampled for radiocarbon dating (Fig. 4). The bottom of the pyroclastic deposit is matrix-rich, whereas the top is matrix-poor. The pyroclastic flow deposit

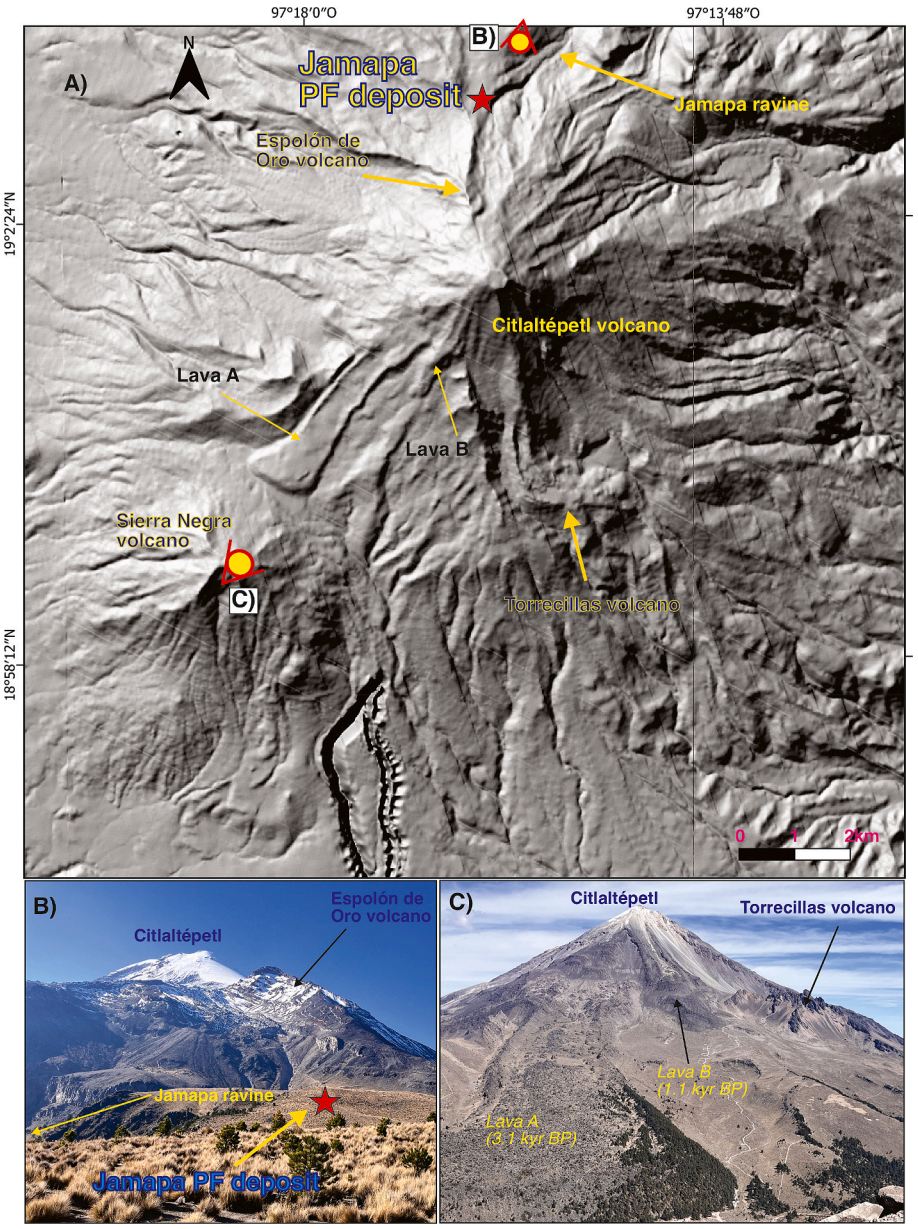

Fig. 3. A) Digital elevation model of the Citlaltépetl volcano, showing the two remnants of previous edifices and the location of the Jamapa Pyroclastic Flow outcrops. The star is the sampled outcrop (see Fig. 4). B) Photograph taken from the north showing the remnant Espolón de Oro volcano. C) Photograph taken from the SW showing the Torrecillas volcano remnant. Places of B and C) panoramic views are indicated in the digital elevation model.

is only overlayed by a reworked material, with irregular thickness (30–50 cm thick), containing fine lapilli clasts of scoria, pumice, and dense blocks (like the pyroclastic deposit) in an ash matrix. The whole sequence of the outcrop rests on a substrate made of andesitic lava flows (Fig. 3) from the Espolón de Oro edifice (Carrasco-Núñez, 2000).

4.1. Age of the Jamapa pyroclastic density current

Unfortunately, we did not find charcoal samples in the deposit, probably because no trees grew at high altitudes (4200 masl) and during the eruption there were no organic matter to burn. Hence, the dark brown paleosol that underlies the Jamapa pyroclastic deposit was sampled and analyzed for radiocarbon dating using the AMS technique. Additional details regarding the analytical procedure and instrumentation are available on the laboratory website (https://www.radiocarbon.com/beta-lab.htm). The sample yielded a conventional radiocarbon age of 5320 ± 30 years before present (BP), which means the deposit should be younger than this age (Table 1).

4.2. Petrologic characteristics

The Jamapa Pyroclastic Flow deposit is constituted mainly by pumice, banded fragments, and scoriaceous fragments of >10 cm in diameter (Fig. 5A-B). In lesser proportion, there are fragments of dense volcanic bombs, with bread-crust structure and crystalline dense fragments defined here as “co-magmatic enclaves” (Fig. 5C-D). At the bottom of the deposit, these fragments are set in an ash matrix while in the upper part of the deposit the ash matrix is almost absent (Fig. 4A).

Under the microscope, the pumice sample is porphyritic, with microphenocrysts (0.03 to 0.3 mm) and phenocrysts (>0.3 mm) of (in order of abundance) plagioclase + ortho- and clinopyroxene, as well as Fe-Ti oxides, in a glassy and vesicular matrix (Fig. 6). Traces of amphibole can be seen. Plagioclase is subhedral to anhedral in shape, some crystals have complex zoning, and therefore, core and rim

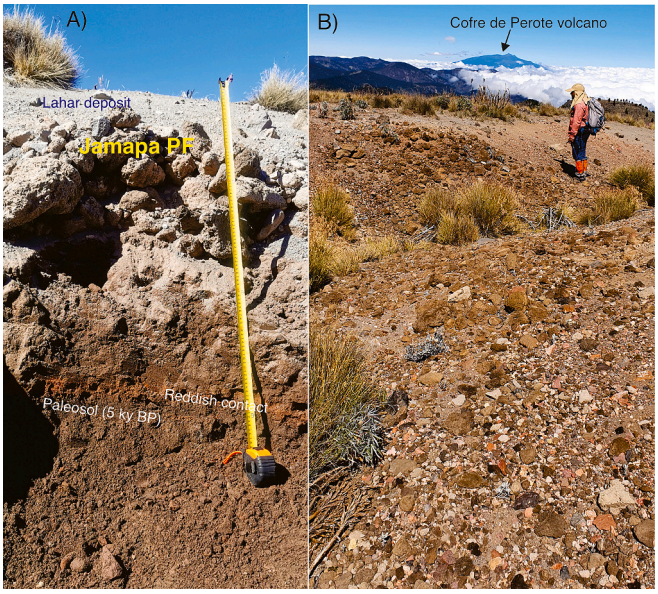

Fig. 4. A) Photograph of a profile of the Jamapa pyroclastic density current deposit on a dark-brown paleosol and covered by a lahar deposit. At the base, the pyroclastic flow deposit is rich in fine ash, while blocks become abundant toward the top. B) Photograph of the surface of the Jamapa pyroclastic density current deposit. Notice the different colors representing different components. (For interpretation of the references to color in this figure legend, the reader is referred to the web version of this article.)

Table 1
Radiocarbon analysis of the paleosol underneath the Jamapa pyroclastic flow deposit.

Sample	Material	Lab Code	C-14 age BP	Cal yr BP	$\delta^{13}C$
CIT-14	Paleosol	Beta - 621,922	5320 ±30	6198–5997	−26.3 o/oo

Analytical details can be seen in the Beta Analyctic Inc. (https://www.radiocarbon.com/sending-carbon-dating-samples.htm).
Conventional and calibrated (cal) ages are reported before present (BP).

compositions are heterogeneous (core composition of An_{30} to An_{59} and rim composition of An_{26} to An_{60} and overlap each other (Fig. 7A and Supplementary Material Table 1; labradorite to oligoclase). Ortho (Wo_3-En_{63}-Fe_{34}) and clinopyroxene (Wo_{43}-En_{40}-Fe_{16}) are homogeneous in composition, even for some glomerocrysts observed in the sample (Fig. 7B; Supplementary Material Table 2).

Scoria samples are porphyritic with phenocrysts and microphenocrysts of plagioclase, amphibole, orthopyroxene, clinopyroxene, and Fe-Ti oxides, set in a glassy and vesicular matrix (Fig. 6). Glomerocrysts of plagioclase and pyroxene are common. Plagioclase crystals exhibit complex zoning and display morphologies ranging from subhedral to anhedral. Their compositions are heterogeneous, with core values varying from An_{33} to An_{82} and rim compositions ranging from An_{27} to An_{78} (Fig. 7A; Suppl. Mat. Table 1). Amphibole phenocrysts are subhedral to anhedral, with a homogeneous composition (ferroan-pargasite-hornblende) either in cores or rims (Suppl. Mat. Table 3). Pyroxene is also homogeneous in composition. Clinopyroxene was classified as augite (Wo_{43}-En_{42}-Fe_{15}), whereas orthopyroxene is enstatite (Wo_2-En_{66}-Fe_{32}).

Banded (pumice and scoria) samples are porphyritic, with phenocrysts of plagioclase + amphibole + pyroxene ± Fe-Ti oxides set in a glassy and vesicular matrix (Fig. 6). Plagioclase is mainly subhedral with complex zoning and heterogeneous composition in cores (An_{29} to An_{77}) and rims (An_{24} to An_{76}) (Fig. 7; Suppl. Mat. Table 1). Pyroxene is mainly subhedral, with compositions of Wo_{42}-En_{39}-Fe_{19} in cores and Wo_{43}-En_{41}-Fe_{16} in rims for clinopyroxene. Orthopyroxene varies from Wo_2-En_{17}-Fe_{27} in cores to Wo_2-En_{71}-Fe_{27} in rims (Fig. 7B; Suppl. Mat. Table 2). Amphibole crystals are mainly subhedral, with a homogeneous composition (Suppl. Mat. Table 3), mainly ferroan-pargasite-hornblende.

The dense volcanic bomb sample is porphyritic, with phenocrysts of plagioclase + ortho- and clinopyroxene + amphibole ± quartz ± Fe-Ti oxides, rare biotite, and olivine, set in a glassy and microlithic matrix (Fig. 6).

Plagioclase is subhedral, some crystals exhibit sieve-texture and corroded margins. Compositional zoning is evident, with core compositions of $An_{35–43}$, inner zones $An_{37–55}$, and rims $An_{39–46}$ (Fig. 7A; Suppl. Mat. Table 1). Ortho- and clinopyroxene are homogeneous in composition with cores of Wo_3-En_{65}-Fe_{32} and rims Wo_3-En_{64}-Fe_{33} (Fig. 7B; Suppl. Mat. Table 2) for orthopyroxene, and Wo_{41}-En_{41}-Fe_{17} in cores; Wo_{42}-En_{41}-Fe_{17} in rims for clinopyroxene. Some amphibole pseudomorphs with clinopyroxene reaction rims are also observed. Quartz varies from 0.27 to 0.30 mm in diameter and commonly has pyroxene reaction rims (Fig. 6). Biotite is rare and commonly shows anhedral shapes. Olivine is very rare, and is present as small fragments, apparently in disequilibrium with the melt.

Magmatic enclaves have a phaneritic texture (Fig. 6G-H), constituted by phenocrysts and microphenocrysts of plagioclase + orthopyroxene + clinopyroxene + amphibole ± Fe-Ti oxides and apatite as accessory mineral. Plagioclase is anhedral to euhedral, with heterogeneous composition, for both cores and rims varying from An_{24} to An_{48}, and An_{31} to An_{61}, respectively (Fig. 7A; Suppl. Mat. Table 1). Amphibole varies from subhedral to anhedral shape, sometimes with reaction rims, and in some cases is totally replaced by oxides (pseudomorphs). Analyzed amphiboles are homogeneous, ranging from ferro-pargasite to edenite-hornblende. Orthopyroxene and clinopyroxene crystals commonly are present as glomerocrysts along with plagioclase crystals with homogeneous composition, from Wo_{42}-En_{42}-Fe_{16} in cores and Wo_{41}-En_{41}-Fe_{18} in rims for Cpx, and Wo_2-En_{64}-Fe_{33} in cores to Wo_3-En_{66}-Fe_{32} in rims for Opx (Fig. 7B; Suppl. Mat. Table 2).

4.3. Chemical composition

Chemical composition of the Jamapa Pyroclastic Flow deposit is heterogeneous (Fig. 8) with the scoria representing the mafic end-member (58.3 to 60.0 wt% SiO_2; all values reported on anhydrous basis), and pumice (62.98 to 63.4 wt% SiO_2) the dacitic member. Banded fragments fall between scoria and pumice compositions (58.42 to 60.16 wt% SiO_2). The dense volcanic bomb is andesitic with 61.12 to 62.14 wt% SiO_2 content, whereas magmatic enclaves are heterogeneous, ranging from 59.67 to 63.35 wt% SiO_2 (Table 2), but all lie in the calc-alkaline series. Glass matrix composition for all samples is heterogeneous (Table 3), ranging from dacite to rhyolite (66.5 to 76.5 wt% SiO_2; Fig. 8), overlapping the bulk composition of the scoria and pumice samples.

By comparing our data with previous results, the Jamapa Pyroclastic Flow deposit falls into the area displayed by previous chemical data (Cantagrel et al., 1984; Siebe et al., 1993; Carrasco-Núñez and Rose, 1995). Major element data shows normal trends for calc-alkaline rocks with negative (Fe_2O_3, CaO, TiO_2, and MgO) and positive (Al_2O_3, Na_2O, and K_2O) trends with increasing SiO_2. Magmatic enclaves (samples Gr-A and Gr-B) and the dense volcanic bomb behave differently; their Na_2O and P_2O_5 contents are high, while K_2O is low, suggesting that these components are not genetically related to the Jamapa Pyroclastic Flow deposit.

Trace element composition of the Jamapa Pyroclastic Flow deposit displays a descending pattern from most incompatible to less incompatible elements. The negative anomalies in Nb, Ta, and Th, to a lesser extent (Fig. 8B), as well as positive anomalies in Ba, Pb, U, Sr, and K are typical characteristics of arc-related magmatism (Pearce, 1982). Dense volcanic bomb samples and magmatic enclaves differ from those

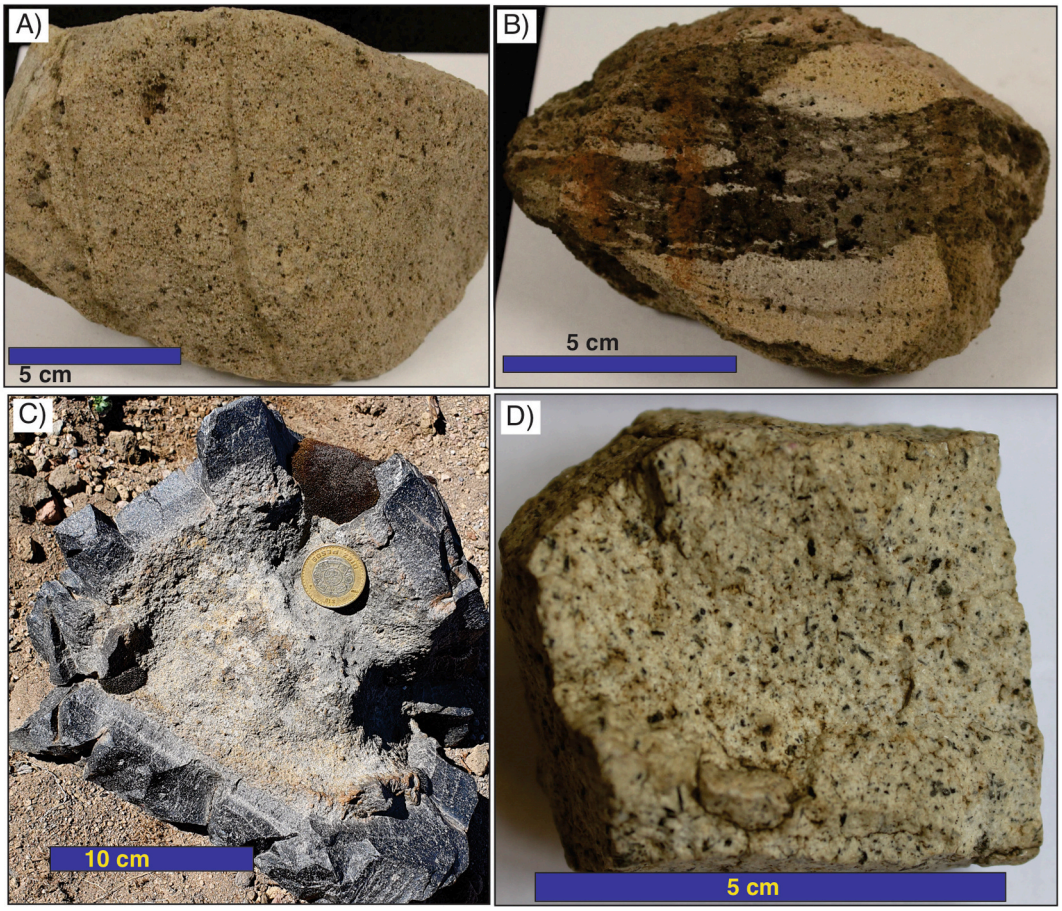

Fig. 5. Constituents of the Jamapa Pyroclastic Flow deposit. A) Ligh-gray and vesicular pumice fragments; B) Banded and vesicular fragments; C) Dense volcanic bombs with bread-crust structures; D) Dense and totally crystalline lithic fragments (magmatic enclaves).

samples of the Jamapa Pyroclastic Flow deposit, again suggesting they are genetically unrelated.

4.4. Geothermobarometry

Recently, machine learning-based thermobarometry models have been developed, either using liquid (MagMaTaB v.4.0; Weber and Blundy, 2024), clinopyroxene-liquid (Agreda-López et al., 2024), or amphibole (Higgins et al., 2022) crystals. Each phase records the pressure and temperature conditions of its formation. For example, the liquid model that considers matrix glass could represent the last stage of the magma just before eruption. On the contrary, mineral phases could record and preserve different P-T conditions during their ascent to the surface. These geothermobarometers were used to constrain the pressure and temperature of the Jamapa Pyroclastic Flow magma as presented in Table 3 and Supplementary Material Tables 2 and 3.

The graph in Fig. 9 shows the results of our calculations. As expected by their mineral composition, each component of the Jamapa Pyroclastic Flow deposit yielded different pressure-temperature conditions. The scoria sample yielded average conditions of 884 ± 65 °C and 2.0 ± 0.35 kb; the pumice sample 898 ± 29 °C and 2.0 ± 0.2 kb; the banded fragment 934 ± 7 °C and 2.0 ± 0.7 kb, and finally, the dense volcanic bomb yielded 853 ± 62 °C and 2.0 ± 0.5 kb, all of them by using the "MagMaTaB" liquid geothermobarometry of Weber and Blundy (2024). Most of the analyses lie between 1 and 2 kb of pressure and between 880 and 920 °C of temperature. Only the scoria and dense volcanic bomb samples display two populations, one of them with a lower temperature (<800 °C).

By using the cpx-liquid geothermobarometry (Agreda-López et al., 2024), we obtained different results. The scoria sample yielded 900 ± 84 °C and 1.6 ± 0.5 kb; the banded fragment resulted 986 ± 5 °C and 5 ± 1.7 kb; the pumice sample (only two good analyses for clinopyroxene crystals) yielded 930 ± 6 °C and pressures between 4 ± 1.0 kb, whereas the dense volcanic bomb yielded 855 ± 69 °C and 4.0 ± 2.2 kb. Regarding the magmatic enclave, it yielded a higher temperature of 1007 ± 16 °C and pressure of 1.3 ± 0.2 kb. These results show dispersed pressure and temperature values, either below or above 2 kb, and from 800 to 1000 °C.

Finally, by using the amphibole geothermobarometry (Higgins et al., 2022), we obtained the following average results: for the scoria sample a temperature of 946 ± 22 °C and pressure of 2.0 ± 1.0 kb; the banded fragment yielded 970 ± 8 °C and 2.0 ± 0.1 kb, and the magmatic enclave yielded 964 ± 15 °C and 2.0 ± 0.2 kb. Unfortunately, we did not get a good analysis of amphibole for pumice and dense volcanic bomb samples. As displayed in Fig. 9, most of the analyses lie in the 2 kb pressure, and temperature around 950 °C, only some analyses for the scoria and magmatic enclave samples are dispersed.

5. Discussion

5.1. Conditions of the ascending magma

Determining the pressure and temperature of the magmas is crucial to understand the dynamics of volcanic eruptions (Cashman et al., 2017; Petrelli et al., 2020) and geophysical monitoring in active volcanoes, such as the InSAR method employed during the 2011–2012 Cordón Caulle eruption (Jay et al., 2014) where the magma was detected at 6–7 km below the volcano. In fact, by combining different and modern

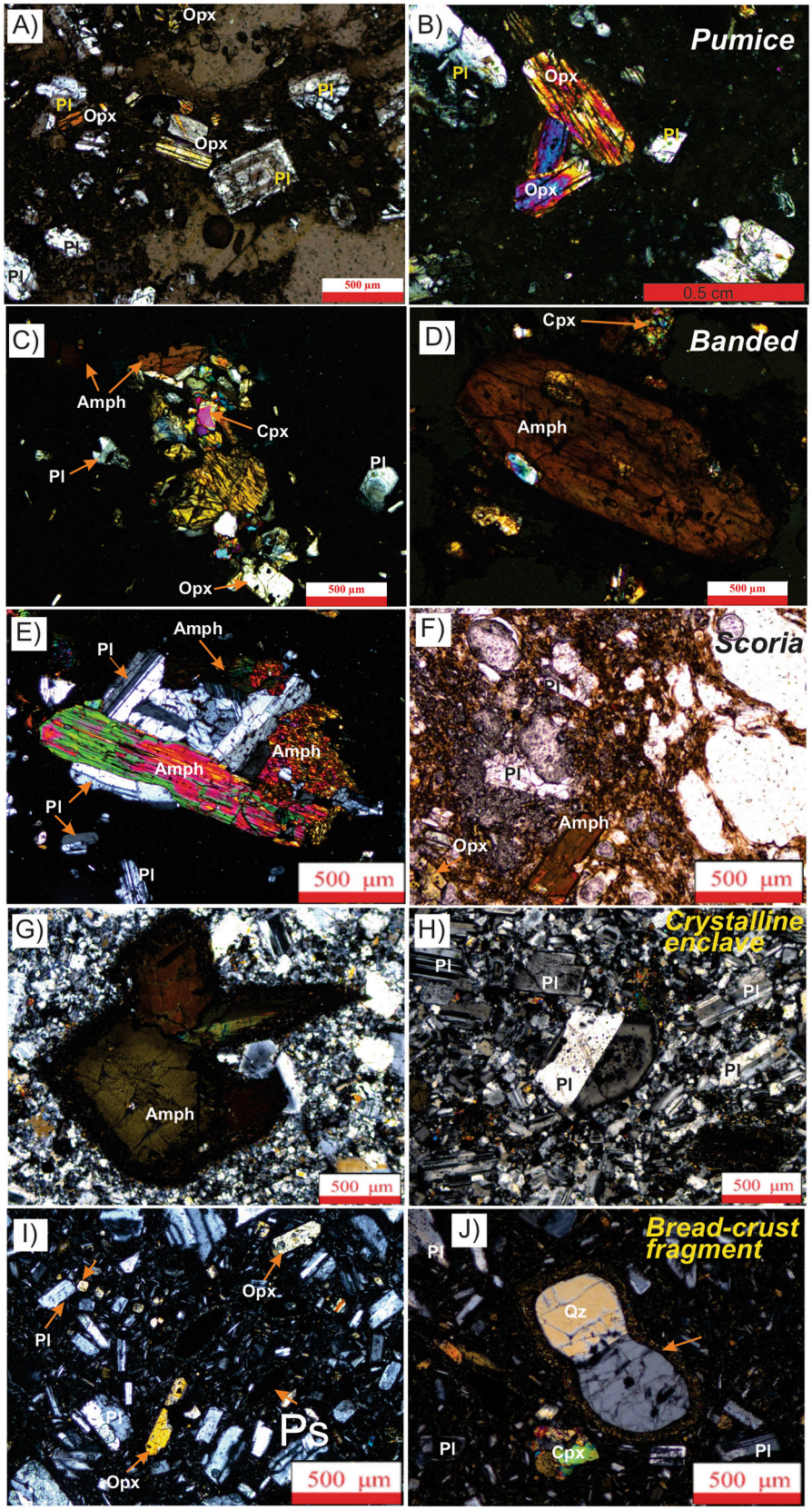

Fig. 6. Microphotographs on cross-polarized light (except F) of the Jamapa Pyroclastic Flow components (scoria, pumice, banded fragment, dense volcanic bomb, and crystalline enclave). Notice some disequilibrium textures (rounded shapes, embayments, and reaction rims), as well as glomerocrysts of pyroxene (Cpx and Opx), amphibole (Amph), and plagioclase (Pl). Quartz (Qz) crystals were found only in the dense volcanic bomb. Fe-Ti oxides (Ox) are common in all samples. The arrow in J) indicates the pyroxene reaction rim on quartz.

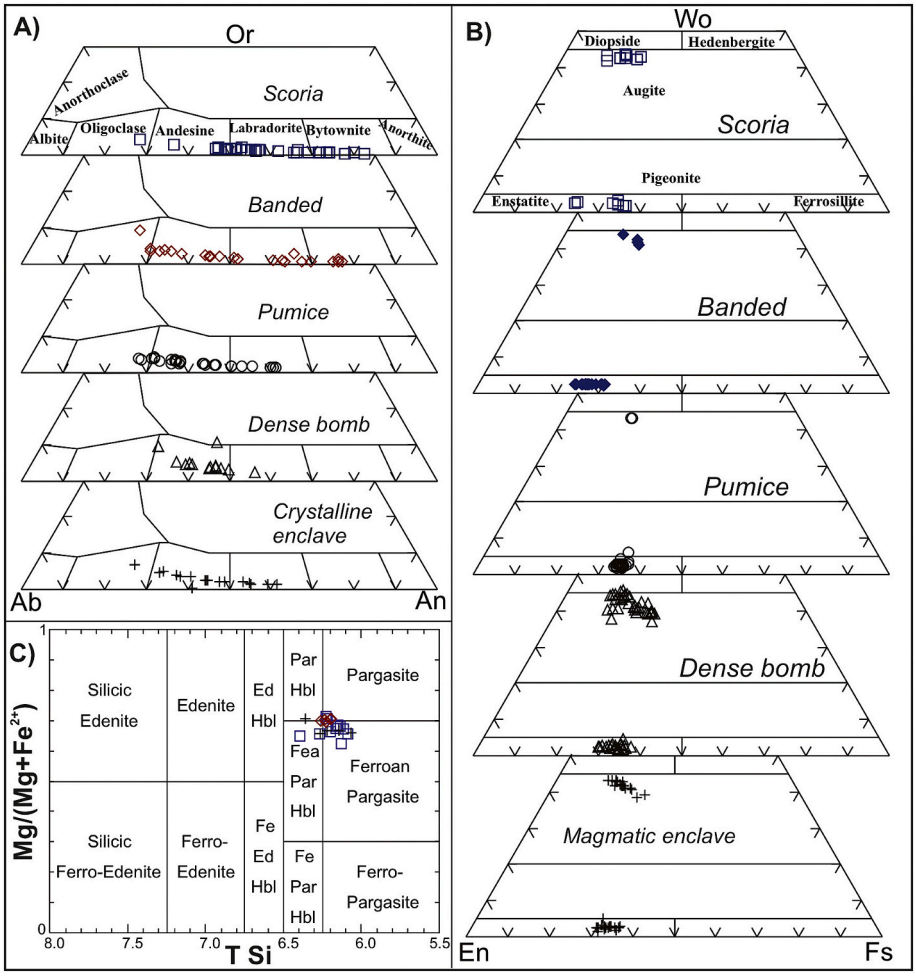

Fig. 7. Ternary diagrams of A) plagioclase, B) pyroxene, and C) amphibole compositions of the Jamapa pyroclastic deposit, showing a large compositional range of plagioclase and homogeneous composition of pyroxene and amphibole.

geophysical techniques it would be possible to track the migration of the magmas below a volcano (Magee et al., 2018). On the other hand, P-T estimations by using different thermobarometers combined with the average density of the crust (2650 kg/m^3) in central Mexico (Ortega-Gutiérrez et al., 2008) allow us to figure out the plumbing system beneath Pico de Orizaba volcano. With these aims in mind, we take the 4500 masl as the 0 km depth (Fig. 10), considering the cone shape and the total altitude of Pico de Orizaba (5636 masl).

Liquid (matrix glass) geobarometry (Weber and Blundy, 2024) results suggest the presence of a well-constrained reservoir around ~8 km beneath the volcano (Table 3; Fig. 10A) with an average temperature of 890 °C for the Jamapa Pyroclastic Flow magma. This depth represents the storage during the last stage of the magma before eruption and coincides with the place of eruptible and felsic magmas proposed for other volcanic systems (Metcalfe et al., 2023). It is possible to use whole-rock chemistry with this liquid geobarometer to figure out the magma source if the magma did not suffer mineral separation or magma mixing (Weber and Blundy, 2024). This is not the case of the Jamapa samples, however, a roughly estimation yielded a depth of ~22 km (Fig. 10A), consistent with the Cpx-liquid geobarometer (see below).

Amphibole geobarometry yielded depths between 10 and 8 km (Suppl. Mat. Table 3; Fig. 10B) for the scoria, banded sample, and the magmatic enclave, with a couple of crystals recording deeper values (the scoria sample). It seems likely that the amphibole was almost in equilibrium with the Jamapa magma that was stored around ~8 km below the volcano (liquid geobarometer; Fig. 10A). Magmatic enclaves crystallized at the same depth as the dacitic and the shallower reservoir.

On the other hand, clinopyroxene-liquid geobarometry yielded variable pressure values (Suppl. Mat Table 2; Fig. 10B). Some data from the scoria and the magmatic enclave magmas recorded shallower depth (less than 6 km) while the pumice and banded samples (as well as the dense volcanic bomb) yielded the deepest values (around 20 km). The depth differences between the mafic and felsic magmas could reflect that both magmas interacted chemically and physically during the mingling/mixing process: the deeper magma was injected into a shallower dacitic magma rese. However, the mixing/mingling mechanism likely interchanged crystals between the andesitic and dacitic melts. The magmatic enclave yielded similar pressure conditions with respect to the Jamapa Pyroclastic Flow samples, suggesting that crystalline bodies (mush-like bodies) are present below the volcano.

The dense volcanic bomb records different pressures (>20 km up to 6 km in depth) that could reflect different stages of clinopyroxene crystallization during the magma ascent. This behavior is different than the rest of the samples of the Jamapa Pyroclastic Flow, suggesting that the dense volcanic bomb could be unrelated to the Jamapa eruption. However, it seems plausible that the two main reservoirs are placed beneath Pico de Orizaba volcano, a deeper one located around 20 km and a shallower one situated at 6–12 km depth (Fig. 10C).

In summary, there seem to be at least two magmatic reservoirs. The deepest one (around 20 km depth) likely corresponding to a relatively mafic, hot, and volatile-rich magma that can feed the shallow, volatile-poor, dacitic magmatic reservoir (~8 km depth).

Table 2
Whole-rock chemical analysis of the Jamapa pyroclastic flow samples.

Sample	PO-2305-A	PO-2305-B	PO-2305-C	CIT 2114a	CIT-2114b	CIT-2114P	CIT-2114P2	CIT-2114Pb	CIT 2114S	Gr A	Gr B
Type	*scoria*	*banded*	*pumice*	*dense*	*dense*	*pumice*	*pumice*	*banded*	*scoria*	*enclave*	*enclave*
SiO2	58.32	58.42	63.40	62.14	61.12	62.98	62.69	60.16	60.07	63.35	59.67
TiO2	0.80	0.76	0.51	0.51	0.67	0.57	0.52	0.72	0.75	0.52	0.65
Al2O3	17.20	17.05	17.41	17.30	16.71	17.39	17.27	17.04	17.09	17.11	17.68
Fe2O3	6.62	6.53	4.36	4.79	5.73	4.40	4.42	5.76	5.88	4.14	6.04
MnO	0.10	0.10	0.08	0.08	0.09	0.08	0.08	0.09	0.09	0.08	0.11
MgO	3.92	3.91	1.87	2.62	3.24	1.98	1.93	3.24	3.29	3.28	3.19
CaO	6.34	6.37	4.43	5.52	5.71	4.59	4.47	5.66	5.93	5.24	5.93
Na2O	3.78	3.66	4.46	4.91	4.07	4.29	4.52	4.07	3.83	4.87	4.68
K2O	1.75	1.81	2.02	1.76	1.96	1.93	1.95	1.91	1.85	1.26	1.79
P2O5	0.20	0.19	0.20	0.26	0.19	0.21	0.19	0.20	0.24	0.20	0.28
LOI	0.99	1.21	1.27	0.11	0.49	1.61	1.76	1.15	1.00	−0.06	−0.01
Total	100.00	100.00	100.00	100.00	100.00	100.01	99.80	100.00	100.02	99.99	#####
Li	11.70	11.94	13.82	13.80	12.67	14.20		12.71	12.66	6.28	10.92
Be	1.50	1.44	1.62	1.63	1.46	1.58		1.53	1.52	1.41	1.45
B	6.35	5.74	6.48	10.85	6.42	18.41		5.89	18.04	3.67	3.46
Sc	14.93	13.79	4.36	11.12	10.42	9.39		10.81	12.15	6.39	10.80
V	149.68	145.26	72.05	133.61	117.48	64.17		119.85	105.21	78.37	#####
Cr	89.96	76.53	40.97	108.32	84.84	10.78		80.94	26.81	52.30	44.76
Co	20.61	20.05	9.12	18.74	16.31	10.44		16.48	16.97	9.10	15.18
Ni	23.78	24.25	8.21	27.81	19.42	9.14		18.87	20.21	12.74	17.93
Cu	40.66	37.43	15.50	34.43	26.13	14.70		30.35	32.79	6.68	6.37
Zn	61.40	59.17	50.15	63.88	55.65	52.20		55.41	58.51	44.60	57.44
Ga	20.06	19.52	19.33	20.65	18.89	20.92		19.44	21.30	20.04	20.57
Rb	37.13	41.55	41.28	57.63	39.53	43.81		39.09	44.29	19.31	32.09
Sr	508.49	515.50	558.79	556.43	497.36	567.51		511.82	540.63	#####	#####
Y	19.56	19.78	14.95	21.54	17.35	14.79		17.59	19.01	14.91	19.09
Zr	172.98	175.40	172.60	218.92	168.01	175.14		176.15	181.74	#####	#####

Sample	PO-2305-A	PO-2305-B	PO-2305-C	CIT 2114a	CIT-2114b	CIT 2114P	CIT-2114Pb	CIT 2114S	Gr A	Gr B
Type	*scoria*	*banded*	*pumice*	*dense*	*dense*	*pumice*	*banded*	*scoria*	*enclave*	*enclave*
Nb	5.77	6.03	5.90	8.59	5.98	5.85	6.13	6.23	5.54	6.19
Mo	1.54	1.36	1.23	2.58	1.68	0.24	1.59	0.31	1.81	1.47
Sn	1.05	0.96	0.82	1.07	0.89	0.79	0.91	0.94	0.58	0.99
Sb	0.15	0.15	0.21	0.20	0.16	0.16	0.16	0.15	0.02	0.05
Cs	1.58	1.62	1.67	2.40	1.64	1.71	1.65	1.78	0.18	0.93
Ba	517.13	543.46	719.18	749.47	600.98	670.28	589.31	576.07	#####	#####
La	20.43	22.49	21.57	27.33	19.77	21.82	19.99	23.06	18.14	19.84
Ce	43.31	44.13	42.38	57.61	40.89	42.49	42.30	45.98	37.88	39.81
Pr	5.54	5.75	5.39	7.13	5.23	5.20	5.37	5.85	4.71	5.01
Nd	22.14	22.67	20.35	27.99	20.50	19.72	20.93	22.85	18.93	20.50
Sm	4.77	4.76	3.98	5.71	4.26	3.92	4.40	4.81	3.86	4.44
Eu	1.26	1.26	1.12	1.46	1.16	1.15	1.14	1.29	1.12	1.30
Tb	0.62	0.62	0.48	0.70	0.55	0.49	0.56	0.61	0.48	0.57
Gd	4.23	4.28	3.38	4.84	3.77	3.57	3.84	4.45	3.30	3.89
Dy	3.52	3.53	2.67	3.71	3.07	2.69	3.14	3.48	2.55	3.13
Ho	0.69	0.69	0.52	0.70	0.60	0.53	0.62	0.68	0.51	0.61
Er	1.89	1.87	1.43	1.84	1.66	1.48	1.71	1.87	1.41	1.62
Yb	1.80	1.78	1.44	1.83	1.57	1.48	1.63	1.80	1.37	1.60
Lu	0.27	0.26	0.22	0.28	0.24	0.22	0.25	0.27	0.21	0.24
Hf	4.45	4.46	4.26	5.38	4.10	4.16	4.45	4.40	3.38	3.62
Ta	0.40	0.41	0.45	0.59	0.72	0.41	0.42	0.43	0.41	0.39
W	2.78	2.17	2.33	2.57	3.16	0.30	2.93	0.57	2.21	2.06
Tl	0.24	0.29	0.35	0.42	0.37	0.31	0.25	0.33	0.03	0.20
Pb	9.50	9.42	10.39	11.29	9.30	10.72	8.78	10.64	8.70	8.41
Th	5.69	5.50	5.07	8.35	5.10	5.32	5.49	6.06	4.64	4.12
U	2.07	2.01	1.73	2.69	1.85	1.92	1.95	2.16	1.43	1.31

Major elements (wt%) determined by XRF and trace elements (ppm) by ICP-MS methods. LOI, loss on ignition; total Fe reported as Fe_2O_3.

5.2. Comparison with other polygenetic Mexican volcanoes

Magmatic plumbing systems in polygenetic volcanoes is currently explained by a transcrustal mush model, where several storage regions can occur (Cashman et al., 2017; Rasmussen et al., 2022) from the base of the crust up to a few km below the volcano. In general, a shallow storage region has been consistently defined in many polygenetic volcanoes at 200 MPa (<10 km depth) and it is the most well defined system because many petrologic and geophysical studies have focused on it (Metcalfe et al., 2023). However, each volcano can record different storage regions, depending on the local tectonics, rheological properties of the magma, and water content (Scaillet et al., 2008; Sparks et al., 2019; Rasmussen et al., 2022).

The Jamapa shallower reservoir around 8 km depth (considering a crustal density of 2560 kg/m^3) coincides with the preferential magma accumulation proposed for many volcanoes around the world, like the Vesuvius volcano (Scaillet et al., 2008). This storage depth (8 km) also coincides with other Mexican volcanic systems (Fig. 11) and it is also considered as the preferential magma accumulation of evolved and eruptible melts (Scaillet et al., 2008). Nevado de Toluca, Popocatépetl, Malinche, and Colima volcanoes record storage depths around 8 km, and only the Jamapa eruption and the 2013–2017 eruptions from Colima

Table 3
Matrix glass composition of the Jamapa pyroclastic flow samples.

Type	Sample	SiO_2	TiO_2	Al_2O_3	FeO	MgO	MnO	CaO	Na_2O	K_2O	Total	T (°C)	P (kb)
	CIT 2114S-1	75.06	0.07	12.84	1.41	0.05	0.07	0.74	5.21	4.38	99.82	771	2.0
	CIT 2114S-2	74.59	0.10	13.17	1.38	0.01	0.07	0.71	4.38	5.12	99.52	788	2.2
	CIT 2114S-3	74.32	0.11	13.22	1.40	0.05	0.06	0.73	4.32	4.97	99.18	798	2.3
	CIT 2114S-4	69.52	0.67	15.57	2.74	1.57	0.04	2.71	4.77	3.19	100.77	934	1.8
Scoria	CIT 2114S-9	68.13	0.72	15.91	3.16	1.79	0.08	2.98	4.53	3.16	100.45	935	2.2
	CIT 2114S-10	67.59	0.72	16.13	2.94	1.77	0.06	2.94	4.55	3.11	99.81	931	2.0
	CIT 2114S-11	74.53	0.45	13.27	1.81	0.55	0.03	1.47	4.07	3.32	99.49	881	1.7
	CIT 2114S-12	73.37	0.54	13.95	1.93	0.81	0.06	1.59	4.56	3.30	100.10	927	1.5
	CIT 2114S-13	73.60	0.52	13.95	1.97	0.80	0.03	1.58	4.62	3.32	100.40	923	1.4
	CIT 2114S-14	73.48	0.49	14.40	1.59	0.73	0.02	1.42	4.95	3.05	100.12	907	1.2
	CIT 2114S-15	69.17	0.64	15.67	2.50	1.38	0.07	2.58	4.87	3.15	100.03	931	1.5
	CIT 2114 PB-2	68.14	0.65	15.99	2.66	1.43	0.07	2.93	5.09	3.01	99.95	926	1.5
	CIT 2114 PB-3	67.88	0.64	15.80	2.47	1.45	0.08	3.20	5.28	3.06	99.85	934	1.8
	CIT 2114 PB-4	65.73	0.67	16.42	2.93	1.43	0.10	2.95	5.08	3.28	98.59	932	1.9
Banded	CIT 2114 PB-5	65.50	0.62	16.08	2.82	1.37	0.10	2.98	2.92	3.00	95.39	931	3.5
	CIT 2114 PB-6	65.24	0.52	15.81	2.19	1.19	0.08	2.40	4.85	3.09	95.37	946	1.6
	CIT 2114 PB-7	67.44	0.66	16.25	2.68	1.37	0.07	2.82	5.84	2.77	99.89	921	1.6
	CIT 2114 PB-8	69.01	0.66	15.59	2.43	0.85	0.02	1.91	4.95	3.46	98.87	934	1.5
	CIT 2114 PB-9	69.02	0.68	15.88	2.76	1.15	0.09	1.85	4.92	3.40	99.74	942	1.5
	CIT 2114 PB-10	68.91	0.66	15.18	2.49	1.17	0.09	2.25	4.85	3.26	98.85	939	1.5
	CIT 2114 PB-11	68.33	0.75	15.31	2.74	1.44	0.07	2.38	3.13	3.28	97.43	938	2.7
	CIT 2114 P-1	66.96	0.68	16.00	2.63	1.56	0.10	2.91	5.42	3.03	99.28	933	1.6
	CIT 2114 P-2	66.07	0.69	15.75	2.54	1.52	0.08	2.76	5.58	3.14	98.13	944	1.5
	CIT 2114 P-3	65.69	0.70	15.56	2.76	1.73	0.05	2.65	5.50	3.28	97.92	946	1.6
	CIT 2114 P-4	72.81	0.42	12.11	1.32	0.53	0.02	0.86	3.17	3.35	94.58	883	1.9
	CIT 2114 P-5	74.33	0.44	11.89	1.46	0.54	0.05	0.96	3.45	3.45	96.58	883	1.6
Pumice	CIT 2114 P-7	74.36	0.41	12.38	1.52	0.50	0.05	1.03	3.51	3.62	97.39	870	1.8
	CIT 2114 P-8	75.48	0.49	12.80	1.51	0.56	0.03	0.97	3.68	3.62	99.13	902	1.6
	CIT 2114 P-9	73.50	0.46	12.39	1.53	0.49	0.04	1.06	3.65	3.62	96.72	885	1.7
	CIT 2114 P-10	76.48	0.44	12.24	1.44	0.51	0.03	1.05	1.95	3.63	97.78	869	1.8
	CIT 2114 P-11	75.10	0.46	12.71	1.60	0.51	0.02	1.11	4.30	3.77	99.58	879	1.5
	CIT 2114 P-12	73.71	0.46	12.52	1.54	0.51	0.03	1.10	2.88	3.70	96.45	881	2.2
	CIT 2114–1	73.67	0.07	13.10	1.44	0.06	0.08	0.73	4.55	5.17	98.87	802	2.7
	CIT 2114–2	73.76	0.09	13.21	1.38	0.04	0.04	0.75	4.67	5.16	99.09	797	2.3
	CIT 2114–3	73.93	0.09	13.17	1.42	0.02	0.08	0.75	4.42	5.09	98.97	791	2.5
Bomb	CIT 2114–4	75.76	0.58	11.82	1.38	0.29	0.02	0.71	3.42	5.25	99.22	911	1.7
	CIT 2114–6	75.01	0.58	11.65	1.38	0.26	0.00	0.61	3.77	5.13	98.39	914	1.5
	CIT 2114–7	74.36	0.50	12.01	1.29	0.29	0.04	0.76	3.88	5.08	98.22	904	1.7

All values reported in wt%, total Fe reported as FeO. Temperature and pressure were calculated with the MagMaTaB liquid model from Weber and Blundy (2024) geothermobarometry. Analytical uncertainties are around 1 %, whereas pressure and temperature is in the order of 1.3 kb and 30 °C respectively as mentioned in the Weber and Blundy (2024) paper.

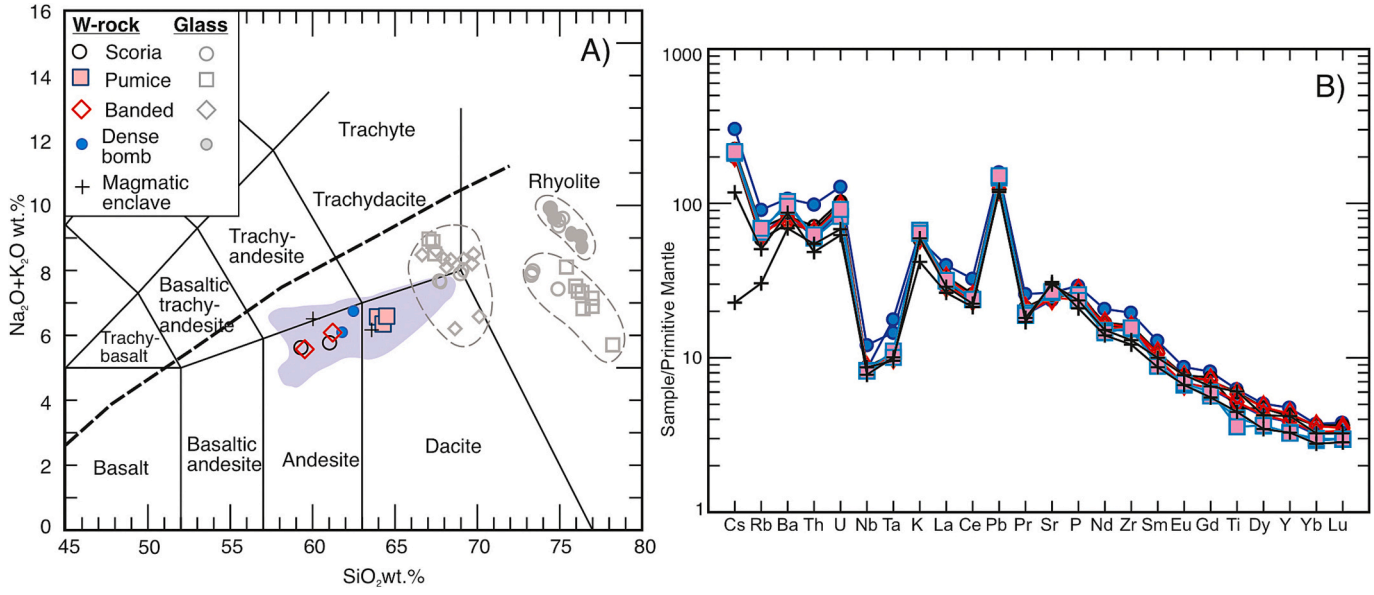

Fig. 8. A) Total alkalis vs. silica diagram of the Jamapa pyroclastic deposit components, showing three groups for glass composition (dashed lines); B) Primitive mantle normalized trace element diagram for the Jamapa Pyroclastic Flow deposit samples, using Sun and McDonough (1989) data.

volcano record deeper (and similar) storage regions around 20 km depth (Fig. 11). Unfortunately, there are no geophysical studies to corroborate

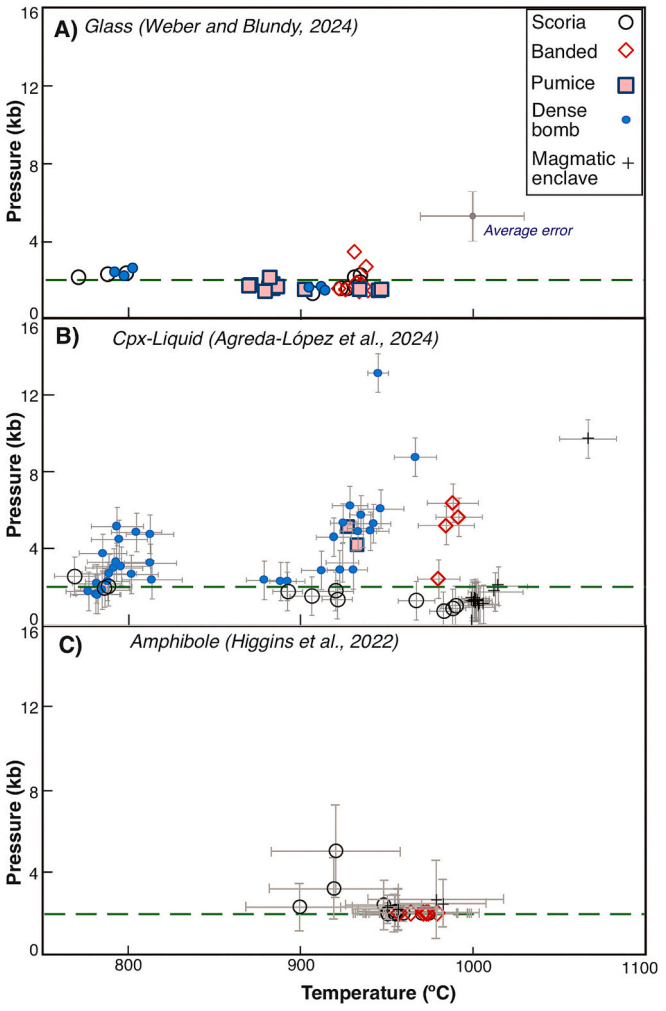

Fig. 9. Pressure and temperature estimations of the Jamapa Pyroclastic Flow samples, using different geothermobarometers. A) MagMaTaB (Weber and Blundy, 2024) of matrix glass of the samples; B) Clinopyroxene-liquid (Agreda-López et al., 2024), being the liquid the average matrix glass composition of each sample; C) Amphibole (Higgins et al., 2022). We included both core and rim compositions because no chemical differences were detected. Error estimations are reported in Table 3 and Suppl. Mat. Tables 2 and 3.

the Jamapa deeper storage system. However, multi-depth magma reservoirs have been documented in other volcanoes around the world like the Lesser Antilles Arc (Metcalfe et al., 2023), hence, the presence of two storage regions in the Pico de Orizaba volcano (and Colima volcano as well) cannot be ruled out.

5.3. Magma mingling/mixing and the eruption

It has been proposed that along the plumbing system, different magmas can interact, either physically, developing banding structures and enclaves; or chemically, detectable only by microanalysis and petrographic observations (reaction rims, heterogeneous rim compositions in plagioclase, large compositional range of matrix glass). These processes can occur either in the reservoirs or during their ascent through the crust (Gansecki et al., 2019; Havard et al., 2025). Magma injection is a very common process in magmatic systems and triggers volcanic eruptions (Morgavi et al., 2022). Mixing is characterized by chemical interactions between two or more magmas producing intermediate compositions, whereas mingling is the physical interaction between two or more magmas (e.g., Jarvis et al., 2021).

In the Jamapa Pyroclastic Flow deposit, we have clear evidence of

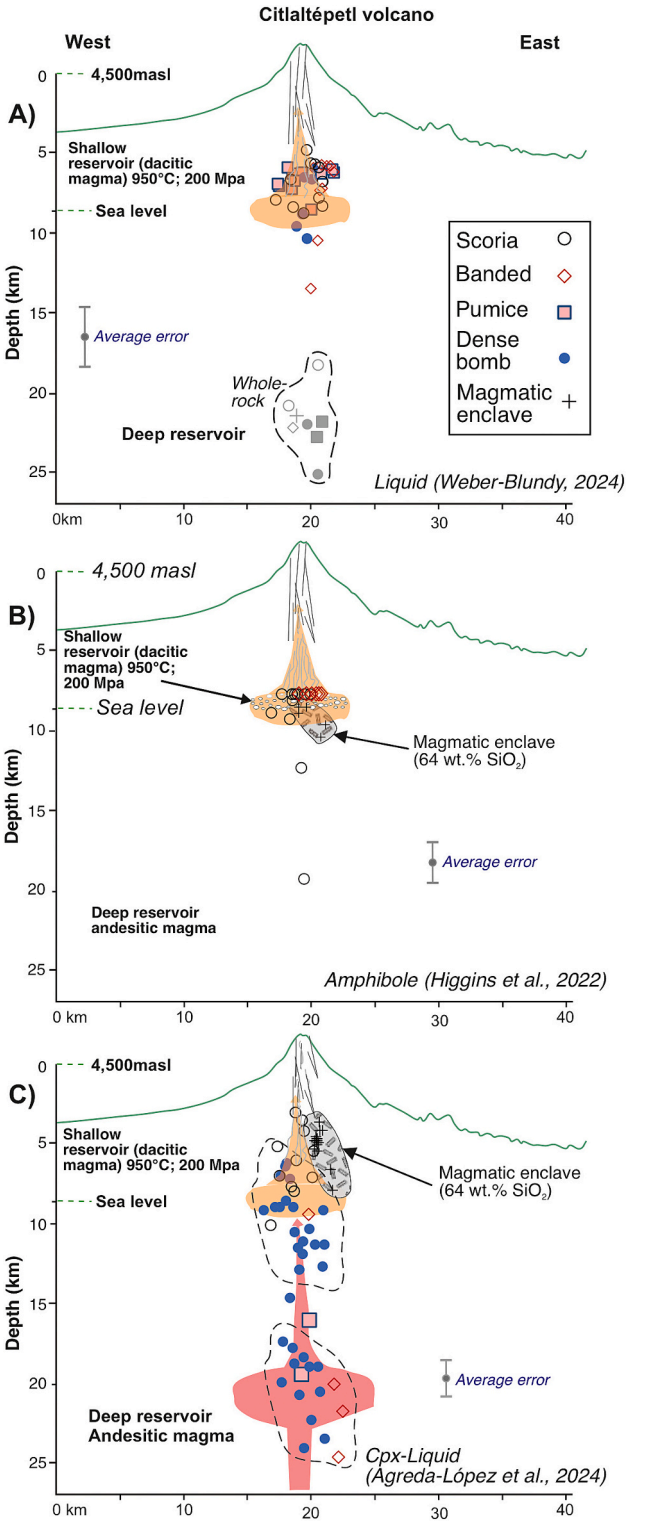

Fig. 10. *E*-W profile and the conceptual model of the magmatic system of Pico de Orizaba volcano around ~5 ky BP. Depth was calculated using the geobarometer results, and an average crustal density of 2650 kg/m^3 was considered for central Mexico (Ortega-Gutiérrez et al., 2008). A) Liquid geothermobarometer (MagMaTaB; Weber and Blundy, 2024); B) Cpx-Liquid geothermobarometer (Agreda-López et al., 2024); C) Amphibole geothermobarometer (Higgins et al., 2022). Considering the three geothermobarometers, it seems that there is a deep reservoir (~20 km) that fed a shallower magmatic reservoir (~8 km) with dacitic melt.

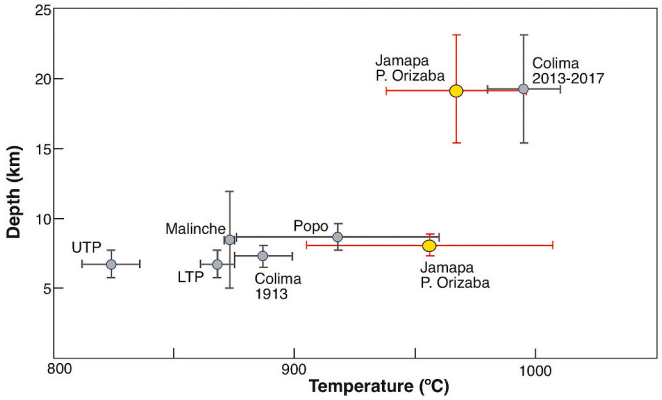

Fig. 11. Depth versus temperature of some magma storage systems of Mexican volcanoes. Error bars indicate the range temperature and pressure reported in previous works. Experimental data for Nevado de Toluca UTP, Upper Toluca Pumice and LTP, Lower Toluca Pumice (Arce et al., 2006; Arce et al., 2013); Popocatépetl Tutti Frutti eruption (Sosa-Ceballos et al., 2014); and 1913 eruption of Colima volcano (Macías et al., 2017), whereas petrologic data are for Malinche volcano (Espinosa et al., 2021) and 2013–2017 eruptions of Colima volcano (Hughes et al., 2021).

mingling. This process is represented by pale pumice, dark scoria, and banded vesicular clasts (Fig. 5), each with different chemical compositions, being the scoria andesitic, the pumice dacitic, and the banded andesitic in composition (Fig. 8). Mineral assemblage is similar (plagioclase + ortho and clinopyroxene, amphibole, Fe-Ti oxides) in each sample (component). Still, they have different proportions, with less amphibole and clinopyroxene in the dacitic pumice sample. However, the matrix glass and the plagioclase composition are heterogeneous (either core and rim compositions) for the three components (scoria, pumice, and banded samples) that overlap each other (Fig. 7). Additionally, these samples have similar pyroxene and amphibole compositions, suggesting that not only mingling, but also mixing between andesitic and dacitic magmas took place.

The dense volcanic bomb could represent an almost solidified andesitic magma, probably from a previous dome structure emplaced before (days or even years) the Jamapa Pyroclastic Flow. The trace element diagram (Fig. 8B) for the dense volcanic bomb displays different concentrations in some elements, plus the different pressure/temperature estimations (Fig. 9). It seems that the magma associated with the dense volcanic bombs corresponds to a magma batch different than the Jamapa Pyroclastic Flow deposit.

On the other hand, the crystalline magmatic enclaves are diverse; some are fine-grained and others coarse-grained, varying from andesite to dacite (Fig. 8A). Mineral assemblage in these enclaves is like the Jamapa pyroclastic components. Furthermore, pressure and temperature estimations are quite similar to the Jamapa components as well (Figs. 9 and 10), suggesting that the enclaves could represent mush-like fragments from different bodies stored and solidified at depth, corresponding to different magma batches.

The Jamapa Pyroclastic Flow is a classic example of magma mixing/mingling related volcanic eruption, like the 1875 Plinian eruption of Askja, Iceland documented many years ago (Sparks et al., 1977), supported by field observations and petrologic data. It seems that this process is a very common phenomena in volcanic systems (Morgavi et al., 2022). Many characteristics support a model where a deep, hot, and gas-rich mafic magma (~20 km depth) arrived at the bottom of the dacitic reservoir (~8 km depth) (Fig. 10B), provoking overpressure of the system that generated vesiculation and eventually fragmentation of the magma to produce the Jamapa explosive eruption, carrying fragments from the conduit and crystalline bodies (mush-like enclaves). It appears that the explosive eruption disrupted a relatively small and solidified dome that had been blocking the conduit. The plug must have been small because no block-and-ash flow deposits were generated during the Jamapa Pyroclastic Flow eruption.

6. Conclusions

The Jamapa pyroclastic density current was produced by an explosive eruption around ~5 ky BP, representing a new eruption that had not been described before in the eruptive chronology of the volcano. The eruption emplaced a scoria and pumice pyroclastic flow deposit on the north flank of Pico de Orizaba volcano (up to 4 km). We propose that mingling and mixing between andesitic and dacitic magmas occurred, supported by the composition of the components (scoria, pumice, and banded scoriaceous fragments), as well as the heterogeneous glass and plagioclase compositions. Thermobarometric results of the Jamapa Pyroclastic Flow samples suggest that an andesitic magma stored at a depth of ~20 km migrated upwards and entered a shallow dacitic reservoir at ~8 km beneath the volcano. Both magmas mingled and mixed, generating overpressure in the system, and at some point, fragmentation occurred. The explosive eruption destroyed a previous relatively small andesitic lava dome, whose components were incorporated in the pyroclastic density current. The mixed magma also incorporated fragments of crystallized bodies from previous magma batches (magmatic enclaves). It is important to perform geophysical studies to compare this data with our findings.

CRediT authorship contribution statement

José Luis Arce: Supervision, Methodology, Investigation, Funding acquisition, Conceptualization. **José Luis Macías:** Writing – review & editing, Resources, Funding acquisition, Data curation. **Mireya González-Herrera:** Methodology, Investigation, Formal analysis, Data curation. **Luca Caricchi:** Visualization, Validation, Software, Conceptualization. **Martin Miranda:** Visualization, Validation, Software, Data curation. **Delphine Sourisseau:** Visualization, Software, Methodology, Data curation. **Denis R. Avellán:** Writing – original draft, Investigation, Data curation. **Rafael Torres-Orozco:** Visualization, Methodology, Formal analysis, Conceptualization.

Funding

This work was supported by DGAPA-UNAM (grants IN-101123 and IN-119523).

Declaration of competing interest

The authors declare that they have no known competing financial interests or personal relationships that could have appeared to influence the work reported in this paper.

Acknowledgements

This research was funded by grants: DGAPA-UNAM IN-101123 (to J. L. Arce) and IN-119523 (to J.L. Macias). FRX analysis was performed at Laboratorio Nacional de Geoquímica y Mineralogía, Instituto de Geología, UNAM by P. Girón-García and ICP-MS analysis was conducted at Instituto de Geociencias, UNAM, Juriquilla, Mexico by O. Pérez Arvizu. Microprobe analysis was performed at Laboratorio Universitario de Petrología, LANGEM-UNAM by C. Linares. Thanks to M.C. Macías-Romo for her help during sample preparation. Thank you very much to K. Németh and J. Roberge for their very constructive and helpful comments that really improved the reading of the final version of the manuscript.

Appendix A. Supplementary data

Supplementary data to this article can be found online at https://doi.org/10.1016/j.lithos.2025.108388.

References

Agreda-López, M., Parodi, V., Musu, A., Jorgenson, C., Carfi, A., Mastrogiovanni, F., Caricchi, L., Perugini, D., Petrelli, M., 2024. En hancing machine learning thermobarometry for clinopyroxene-bearing magmas. Comput. Geosci. 193, 105707. https://doi.org/10.1016/j.cageo.2024.105707.

Alcalá-Reygosa, J., Vázquez-Selem, L., Zamorano, J.J., 2020. Fechamiento de flujos de lava del Holoceno tardío en el volcán Citlaltépetl (Pico de Orizaba) mediante el isótopo cosmogénico 36Cl y liquenometría e implicaciones para la cronología eruptiva. Bol. Soc. Geol. Mex. 72 (1). https://doi.org/10.18268/bsgm2020v72n1a260919.

Arce, J.L., Macías, J.L., Gardner, J., Layer, P., 2006. A 2.5 ka history of dacitic magmatism at Nevado de Toluca, Mexico: petrological, 40Ar/39Ar dating, and experimental constraints on petrogenesis. J. Petrol. 47, 457–479.

Arce, J.L., Gardner, J., Macías, J.L., 2013. Pre-eruptive conditions of dacitic magma erupted during the 21.7 ka Plinian event at Nevado de Toluca volcano, Central Mexico. J. Volcanol. Geotherm. Res. 249, 49–65. https://doi.org/10.1016/j.jvolgeores.2012.09.012.

Arce, J.L., Ferrari, L., Morales-Casique, E., Vasquez-Serrano, A., Arroyo, S.M., Layer, P. W., Benowitz, J., López-Martínez, M., 2020. Early Miocene arc volcanism in the Mexico City Basin: inception of the Trans-Mexican Volcanic Belt. J. Volcanol. Geotherm. Res. 408, 107104. https://doi.org/10.1016/j.jvolgeores.2020.107104.

Bachmann, O., Bergantz, G.W., 2006. Gas percolation in upper-crustal silicic crystal mushes as a mechanism for upward heat advection and rejuvenation of near-solidus magma bodies. J. Volcanol. Geotherm. Res. 149, 85–102. https://doi.org/10.1016/j.jvolgeores.2005.06.002.

Campos-Enríquez, O., Garduño-Monroy, V.H., 1987. The shallow structure of Los Humeros and Las Derrumbadas geothermal fields, Mexico. Geothermics 16, 539–554. https://doi.org/10.1016/0375-6505(87)90038-1.

Cantagrel, J.M., Gourgaud, A., Robin, C., 1984. Repetitive mixing events and holocene pyroclastic activity at Pico de Orizaba and Popocatepetl (Mexico). Bull. Volcanol. 47 (4), 735–748. https://doi.org/10.1007/BF01952341.

Caricchi, L., Townsend, M., Rivalta, E., Namiki, A., 2021. The build-up and triggers of volcanic eruptions. Nat. Rev.Earth Env. 2, 458–476.

Carrasco-Núñez, G., 2000. Structure and proximal stratigraphy of Citlaltépetl volcano, México. In: Mexico: Special Paper of the Geological Society of America, 334, pp. 247–262. https://doi.org/10.1130/0-8137-2334-5.247.

Carrasco-Núñez, G., Rose, W.I., 1995. Eruption of a major Holocene pyroclastic flow at Citlaltépetl volcano (Pico de Orizaba), México, 8.5–9.0 ka. J. Volcanol. Geotherm. Res. 69 (3–4), 197–215. https://doi.org/10.1016/0377-0273(95)00023-2.

Carrasco-Núñez, G., Vallance, J.W., Rose, W.I., 1993. A voluminous avalanche-induced lahar from Citlaltépetl volcano, Mexico: implications for hazard assessment. J. Volcanol. Geotherm. Res. 59, 35–46. https://doi.org/10.1016/0377-0273(93)90076-4.

Carrasco-Núñez, G., Hernández, J., Cavazos-Álvarez, J., Norini, G., Orozco-Esquivel, T., López-Quiroz, P., Jáquez, A., De León-Barragán, L., 2021. Volcanic geology of the easternmost sector of the Trans-Mexican Volcanic Belt, Mexico. J. Maps 17 (2), 474–484. https://doi.org/10.1080/17445647.2021.1970037.

Cashman, K.V., Giordano, G., 2014. Calderas and magma reservoirs. J. Volcanol. Geotherm. Res. 288, 28–45. https://doi.org/10.1016/j.jvolgeores.2014.09.007.

Cashman, K.V., Sparks, R.S.J., Blundy, J.D., 2017. Vertically extensive and unstable magmatic systems: a unified view of igneous processes. Science 355 (6331), eaag3055. https://doi.org/10.1126/science.aag3055.

Cioni, R., Pistolesi, M., Pompilio, M., Scaillet, B., 2021. Understanding volcanic systems and their dynamics combining field and physical volcanology with petrology studies. In: Forecasting and Planning for Volcanic Hazards, Risks, and Disasters, 2, pp. 285–328. https://doi.org/10.1016/B978-0-12-818082-2.00007-X.

Cooper, K.M., Kent, A.J.R., 2014. Rapid remobilization of magmatic crystals kept in cold storage. Nature 506, 480–483. https://doi.org/10.1038/nature12991.

Crausaz, W., 1994. Pico de Orizaba O Citlaltépetl: Geology, Archaeology, History, Natural History and Mountaineering Routes. Geopress International, Ohio, p. 594.

Doocy, S., Daniels, A., Dooling, S., Gorokhovich, Y., 2013. The human impact of volcanoes: a historical review of events 1900-2009 and systematic literature review. PLoS Curr. 5. https://doi.org/10.1371/currents.dis.841859091a706efebf8a30f4ed7a1901, 2013 Apr 16.

Eichelberger, J.C., Izbekov, P.E., 2000. Eruption of andesite triggered by dyke injection: contrasting cases at Karymsky volcano, Kamchatka and Mt Katmai, Alaska. Philos. Trans. R. Soc. Lond. A 358, 1465–1485. https://www.jstor.org/stable/2666924.

Espinosa, V.D., Arce, J.L., Cstro-Govea, R., 2021. Pre-eruptive conditions and reheating of dacitic magma (Malinche Pumice II Plinian eruption) at La Malinche volcano, Central Mexico. J. Volcanol. Geotherm. Res. 419, 107368. https://doi.org/10.1016/j.jvolgeores.2021.107368.

Ferrari, L., Orozco-Esquivel, T., Manea, V., Manea, M., 2012. The dynamic history of the Trans-Mexican Volcanic Belt and the Mexico subduction zone. Tectonophysics 522, 122–149. https://doi.org/10.1016/j.tecto.2011.09.018.

Gansecki, C., Lee, R.L., Shea, T., Lundblad, S.P., Hon, K., Parcheta, C., 2019. The tangled tale of Kilauea's 2018 eruption as told by geochemical monitoring. Science 366 (6470). https://doi.org/10.1126/science.aaz0147.

Gómez-Alvarez, F., Garduño-Monroy, V.H., Sosa-Ceballos, G., Jiménez-Haro, A., Liotta, D., Gaitan-Ramírez, M.F., Brogi, A., Israde-Alcántara, I., Nájera-Blas, S.M., Wheeler, W., Forster, M., García-Hernández, O.H., 2021. New constraints on tectonism and magmatism from the eastern sector of the Trans-Mexican Volcanic Belt (Chignahuapan horst, Puebla, Mexico). J. S. Am. Earth Sci. 112, 103468. https://doi.org/10.1016/j.jsames.2021.103468.

Gómez-Tuena, A., Langmuir, C.H., Goldstein, S.L., Straub, S.M., Ortega- Gutiérrez, F., 2007. Geochemical evidence for slab melting in the Trans-Mexican Volcanic Belt. J. Petrol. 48, 537–562.

Gueugneau, V., Kelfoun, K., Charbonnier, S., Germa, A., Carazzo, G., 2020. Dynamics and impacts of the May 8th, 1902 Pyroclastic current at Mount Pelée (Martinique): new insights from numerical modeling. Front. Earth Sci. 8, 279. https://doi.org/10.3389/feart.2020.00279.

Havard, T.A., Jones, T.J., Kavanagh, J.L., 2025. Analogue experiments to investigate magma mixing within dykes. Bull. Volcanol. 87, 29. https://doi.org/10.1007/s00445-025-01809-0.

Higgins, O., Sheldrake, T., Caricchi, L., 2022. Machine learning thermobarometry and chemometry using amphibole and clinopyroxene: a window into the roots of an arc volcano (Mount Liamuiga, Saint Kitts). Contrib. Mineral. Petrol. 177 (1), 1–22. https://doi.org/10.1007/s00410-021-01874-6.

Höskuldsson, A., Robin, C., 1993. Late Pleistocene to Holocene eruptive activity of Pico de Orizaba, Eastern Mexico. Bull. Volcanol. 55 (8), 571–587. https://doi.org/10.1007/BF00301810.

Huber, C., Bachmann, O., Dufek, J., 2011. Thermo-mechanical reactivation of locked crystal mushes: melting-induced internal fracturing and assimilation processes in magmas. Earth Planet. Sci. Lett. 304, 443–454. https://doi.org/10.1016/j.epsl.2011.02.022.

Hughes, G.E., Petrone, C.M., Downes, H., Varley, N.R., Hammond, S.J., 2021. Mush remobilization and mafic recharge: a study of the crystal cargo of the 2013-17 eruption at Volcán de Colima, Mexico. J. Volcanol. Geotherm. Res. 416, 107296. https://doi.org/10.1016/j.jvolgeores.2021.107296.

Jarvis, P.A., Pistone, M., Secretan, A., Blundy, J.D., Cashman, K.V., Mader, H.M., Baumgartner, L.P., 2021. Crystal and volatile controls on the mixing and mingling of magmas. In: Crustal Magmatic System Evolution: Anatomy, Architecture, and Physico-Chemical Processes, pp. 125–150.

Jay, J., Costa, F., Pritchard, M., Lara, L., Singer, B., Herrin, J., 2014. Locating magma reservoirs using InSAR and petrology before and during the 2011-2012 Cordón Caulle silicic eruption. Earth Planet. Sci. Lett. 395, 254–266. https://doi.org/10.1016/j.epsl.2014.03.046.

Lenhardt, N., Böhnel, H., Wemmer, K., Torres-Alvarado, I.S., Hornung, J., Hinderer, M., 2010. Petrology, magnetostratigraphy and geochronology of the Miocene volcaniclastic Tepoztlán Formation: implications for the initiation of the Transmexican Volcanic Belt (Central Mexico). Bull. Volcanol. 72, 817–832. https://doi.org/10.1007/s00445-010-0361-z.

Luongo, G., Perrotta, A., Scarpati, C., De Carolis, E., Patricelli, G., Ciarallo, A., 2003. Impact of the AD 79 explosive eruption on Pompeii, II. Causes of death of the inhabitants inferred by stratigraphic analysis and areal distribution of the human casualties. J. Volcanol. Geotherm. Res. 126, 169–200. https://doi.org/10.1016/S0377-0273(03)00147-1.

Macías, J.L., Sosa-Ceballos, G., Arce, J.L., Gardner, J.E., Saucedo, R., Valdez-Moreno, G., 2017. Storage conditions and magma processes triggering the 1818 CE Plinian eruption of Volcán de Colima. J. Volcanol. Geotherm. Res. 340, 117–129. https://doi.org/10.1016/j.jvolgeores.2017.02.025.

Magee, C., Stevenson, C.T., Ebmeier, S.K., Keir, D., Hammond, J.O., Gottsmann, J.H., Jackson, M.D., 2018. Magma plumbin systems: a geophysical perspective. J. Petrol. 59 (6), 1217–1251. https://doi.org/10.1093/petrology/egy064.Mooser et al., 1958.

Metcalfe, A., Moune, S., Komorowski, J.-C., Robertson, R., Christopher, T.E., Joseph, E. P., Moretti, R., 2023. Diverse magma storage and major and volatile magma composition: what are the implications on the eruptive style across a volcanic arc? An example of the Lesser Antilles Arc. Earth Sci. Rev. 241, 104440. https://doi.org/10.1016/j.earscirev.2023.104440.

Mooser, F., Meyer-Abich, H., McBirney, A.R., 1958. Catalogue of the Active Volcanoes of the World Including Solfatara Fields, 6. International Volcanological Association, Part VI Central America, pp. 144–145.

Morgavi, D., Laumonier, M., Petrelli, M., Dingwell, D.B., 2022. Decrypting magma mixing in igneous systems. Rev. Mineral. Geochem. 87 (1), 607–638. https://doi.org/10.2138/rmg.2022.87.13.

Mori, L., Gómez-Tuena, A., Cai, Y., Goldstein, S.L., 2007. Effects of prolonged flat subduction on the Miocene magmatic record of the central Trans-Mexican Volcanic Belt. Chem. Geol. 244, 452–473.

Nielsen, C.H., Sigurdsson, H., 1981. Quantitative methods for electron microprobe analysis of sodium in natural and synthetic glasses. Am. Mineral. 66, 547–552.

Ortega-Gutiérrez, F., Elías-Herrera, M., Dávalos-Elizondo, M.G., 2008. On the nature and role of the lower crust in the volcanic front of the Trans-Mexican Volcanic Belt and its fore-arc region, southern and Central México. Revista Mexicana de Ciencias Geológicas 25, 346–364.

Pearce, J.A., 1982. Trace element characteristics of lavas from destructive plate boundaries. In: Thorpe, R.S. (Ed.), Andesites; Orogenic Andesites and Related Rocks, 1982. Wiley, New York, pp. 524–548.

Pérez-Campos, X., Kim, Y.H., Husker, A., Davis, P.M., Clayton, R.W., Iglesias, A., Pacheco, J.F., Singh, S.K., Manea, V.C., Gurnis, M., 2008. Horizontal subduction and truncation of the Cocos Plate beneath Central Mexico. Geophys. Res. Lett. 35 (18). https://doi.org/10.1029/2008GL035127.

Petrelli, M., Caricchi, L., Perugini, D., 2020. Machine learning thermo-barometry: application to clinopyroxene-bearing magmas. J. Geophys. Res. Solid Earth 125 (9). https://doi.org/10.1029/2020JB020130.

Rasmussen, D.J., Plank, T.A., Roman, D.C., Zimmer, M.M., 2022. Magmatic water content controls the pre-eruptive depth of arc magmas. Science 375, 1169–1172. https://doi.org/10.1126/science.abm5.

Rossotti, A., Carrasco-Núñez, G., 2004. Stratigraphy of 8.5-9 ka B.P. Citlatépetl pumice fallout sequence. Revista Mexicana de Ciencias Geológicas 21 (3), 353–370.

Scaillet, B., Pichavant, M., cioni, R., 2008. Upward migration of Vesuvius magma chamber over the past 20,000 years. Nature 455, 216–219. https://doi.org/10.1038/nature07232.

Schaaf, P., Carrasco-Núñez, G., 2010. Geochemical and isotopic profile of Pico de Orizaba (Citlaltépetl) volcano, Mexico: insights for magma generation processes. J. Volcanol. Geotherm. Res. 197 (1–4), 108–122. https://doi.org/10.1016/j.jvolgeores.2010.02.016.

Siebe, C., Abrams, M., Sheridan, M.F., 1993. Major Holocene block-and-ash fan at the western slope of ice-capped Pico de Orizaba volcano, México: implications for future hazards. J. Volcanol. Geotherm. Res. 59 (1–2), 1–33. https://doi.org/10.1016/0377-0273(93)90075-3.

Sosa-Ceballos, G., Gardner, J.E., Lassiter, J.C., 2014. Intermittent mixing processes occurring before Plinian eruptions of Popocatepetl volcano, Mexico: insights from textural-compositional variations in plagioclase and Sr-Nd-Pb isotopes. Contrib. Mineral. Petrol. 167, 966. https://doi.org/10.1007/s00410-014-0966-x.

Sparks, R.S.J., Sigurdsson, H., Wilson, L., 1977. Magma mixing: a mechanism for triggering acid explosive eruptions. Nature 267, 315–318.

Sparks, R.S.J., Annen, C., Blundy, J.D., Cashman, K.V., Rust, A.C., Jackson, M.D., 2019. Formation and dynamics of magma reservoirs. Phil. Trans. R. Soc. A 377 (2139), 20180019.

Sun, S.S., McDonough, W.F., 1989. Chemical and isotopic systematics of oceanic basalts: implications for mantle composition and processes. Geol. Soc. Lond. Spec. Publ. 42 (1), 313–345. https://doi.org/10.1144/GSL.SP.1989.042.01.19.

Vásquez-Montoya, M., Torres-Orozco, R., Arce, J.L., Sieron, K., Córdoba-Montiel, F., 2025. Unraveling recurrent Pleistocene-Holocene multiphase explosive eruptions of Pico de Orizaba (Citlaltépetl), Mexico, from lithostratigraphic analysis and radiocarbon dating. J. Volcanol. Geotherm. Res. https://doi.org/10.1016/j.jvolgeores.2025.108384, 108384.

Weber, G., Blundy, J., 2024. A machine learning-based thermobarometer for magmatic liquids. J. Petrol. 65, egae020. https://doi.org/10.1093/petrology/egae020.

Yamamoto, T., Nakano, S., Ishizuca, Y., 2021. Temporal variations of magma composition, eruption style and rate at Fuji volcano, Japan. Earth Planets Space 73, 169. https://doi.org/10.1186/s40623-021-01505-1.